Permeation Enhancer-Induced Membrane Defects Assist the Oral Absorption of Peptide Drugs

Kyle J. Colston,[a] *Kyle T. Faivre,*[b] *and Severin T. Schneebeli*[a,b,]*

[a] Department of Industrial & Molecular Pharmaceutics
Purdue University
West Lafayette, IN 47906, USA

[b] James Tarpo Jr. and Margaret Tarpo Department of Chemistry
Purdue University
West Lafayette, IN 47906, USA

* Corresponding Author E-mail: schneebeli@purdue.edu

ABSTRACT

The passive membrane permeation of small-molecule drugs and relatively small hydrophobic peptides is relatively well understood. In contrast, how long polar peptides can directly pass through a membrane has remained a mystery. This process can be achieved with transcellular permeation enhancers, contributing significantly to the oral transcellular absorption of important peptide drugs like semaglutide — the active component in Ozempic, which is used as Rybelsus in a successful oral formulation. Here we now provide, for the first time, a detailed, plausible molecular mechanism of how such a polar peptide can realistically pass through a membrane paired with the permeation enhancer salcaprozate sodium (SNAC). We provide not only simulation results, obtained with scalable continuous constant pH molecular dynamics (CpHMD) simulations, but also experimental evidence (NMR, DOSY, and DLS) to support this unique passive permeation mechanism. Our computational and experimental evidence points toward the formation of permeation-enhancer-filled, fluid membrane defects, in which the polar peptide can be submerged in a process analogous to sinking in quicksand.

INTRODUCTION

In this work, we investigate the fundamental question of how long polar peptides can directly pass through a membrane with the help of permeation enhancers. By advancing toward this general goal, we aim to enhance the mechanistic understanding of oral peptide drug formulations for polar peptide drugs (see Fig. 1C for an example). This knowledge is needed to help guide the rational design of improved oral formulations for such peptides in the future. Our work contrasts with computational permeability studies of small molecule drugs[2] (Fig. 1A) and macrocyclic peptides with mostly hydrophobic side chains[3] (Fig. 1B). For these types of structures, structure-based computational modeling is already able to provide a relatively accurate mechanistic picture of the membrane permeability, especially when coupled with continuous constant pH molecular dynamics (CpHMD) models for small-molecule drugs[2] (Fig. 1A) and sufficient conformational

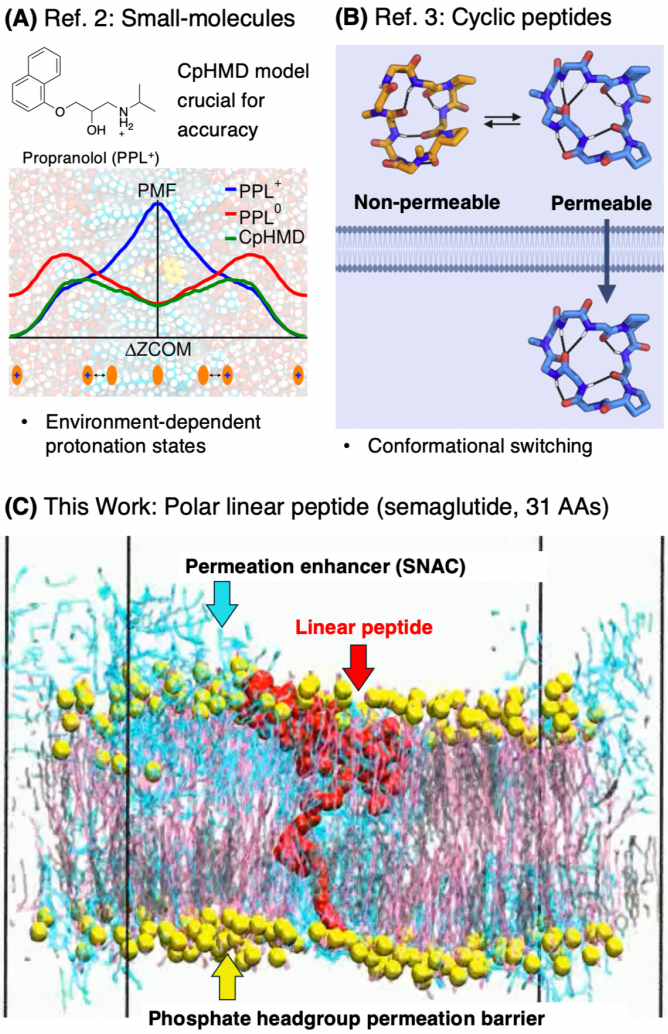

Fig. 1 | Different Types of Passive Membrane Permeation Mechanisms. (A) Permeation of a small-molecule drug with environment-dependent protonation-state switching (Ref. 2). **(B)** Permeation of a macrocyclic peptide drug with nonpolar side chains based on environment-dependent conformational switching (Ref. 3). **(C)** Permeation-enhancer enabled incorporation of a linear, polar peptide drug (this work). Figs. 1A and B were reproduced in parts with permission from Refs. 2 and 3.

sampling for macrocyclic peptides[3] (Fig. 1B). As a result, the passive membrane permeation of small molecules and macrocyclic peptides is reasonably well understood (to the point where rational computational design has become possible[3, 4]). However, in addition to the permeation of small molecules and macrocyclic peptides with mostly nonpolar sidechains, it has recently been discovered[5] that polar, linear peptides like semaglutide can very likely also pass directly through membranes with the help of permeation enhancers like salcaprozate sodium (SNAC, Fig. 2)[6-8]. This new finding cannot be readily explained with the currently available mechanistic models, and it is still mostly unknown how this permeation enhancer-facilitated process occurs. Nevertheless, even without a full understanding of this peptide permeation process, this approach has been adopted by Novo Nordisk to create one of the first successful oral formulations of a long, linear peptide drug (semaglutide), which is widely adopted on the market.[9]

Overall, oral peptide drug formulations are highly desirable because they offer enhanced patient compliance compared to subcutaneous injections[10-13], while also preventing potential overdose

issues that can arise with subcutaneous injections for GLP-1 agonists like semaglutide, which are projected to be used by over 9% of the American population by 2030.[9] However, the development of viable oral peptide formulations has been slow due to the low proteolytic stability and poor intrinsic gastric/intestinal permeability of most peptide drugs. For example, since the 1940s, the field has been striving to develop an oral formulation of insulin, but still, no widely adopted oral formulation has been discovered. For this reason, Novo Nordisks's oral formulation of semaglutide (Rybelsus), which contains 7–14 mg of the peptide drug, co-formulated with ~400 mg of SNAC, represents a remarkable achievement in the oral peptide drug delivery space. Yet, the oral bioavailability of semaglutide with SNAC still remains very low (<1%).[14] At the same time, the understanding of the absorption mechanism with SNAC is still very limited, which has been hindering rational, mechanistically-guided improvements to the current oral formulation of semaglutide.[15-18]

It is currently known that SNAC stabilizes semaglutide in the stomach by inactivating pepsin (which is achieved by increasing the local pH around the tablet[19]). Nevertheless, the detailed molecular mechanism by which SNAC enables semaglutide to permeate the gastric epithelial barrier remains largely unknown. Most experimental evidence suggests[20] a transcellular absorption mechanism, with one of the current theories proposing that SNAC fluidizes the membrane, which then assists semaglutide in passing through the gastric epithelial cells.[18] Although initial computational studies have provided valuable insights into the interactions between SNAC and model membranes,[21, 22] no detailed molecular mechanism for semaglutide permeation has yet been verified. Specifically, it remains unclear how membrane fluidization can facilitate peptide permeation without damaging the epithelial cells. Here, we now describe a viable molecular mechanism for SNAC-enabled peptide permeation of semaglutide. Our results were obtained with accurate, all-atom CpHMD simulations and are supported by experimental evidence obtained in $CDCl_3$ as a well-established model for the hydrophobic membrane interior.[3, 23-25] Notably, in our μs-long CpHMD simulations, we observed semaglutide spontaneously incorporating into the membrane in the presence of the permeation enhancer SNAC, which explains, for the first time, how a long linear, and relatively polar peptide can get past the phospholipid barrier in a membrane in the presence of a permeation enhancer without damaging the integrity of the membrane.

To account for all the weakly ionizable functional groups in our system (with ~400 ionizable

groups in SNAC and 11 in semaglutide), we utilized a scalable CpHMD model implemented in GROMACS.[26] This CpHMD model, which achieved approximately 80% of the performance speed of a regular MD simulation, is essential to provide accurate, environment-dependent pK_a values and environment-dependent charges for the complex peptide/permeation-enhancer/lipid-bilayer interactions in this system. Our simulations revealed a more even distribution of SNAC between the membrane and water layer compared to classical simulations with a fixed protonation state model, enabling SNAC to act as a detergent in the water layer while at the same time facilitating peptide drug permeation within the membrane. Specifically, a 1-μs unbiased CpHMD simulation (likely the largest CpHMD model constructed to date) shows that SNAC aggregates around semaglutide in both the interior and the exterior of the membrane. These aggregates form dynamic, partially fluid SNAC-filled membrane defects that can enable passive semaglutide permeation across the membrane by a mechanism reminiscent of quicksand. Additional support for dynamic SNAC aggregation in nonpolar environments was obtained through CpHMD simulations in CH_2Cl_2, as well as diffusion-ordered spectroscopy (DOSY), NMR titrations, and dynamic light scattering (DLS) experiments in $CDCl_3$, an established mimic of the hydrophobic membrane interior.[3, 23-25] Collectively, these results suggest a new, plausible molecular mechanism for passive membrane permeation with transcellular permeation enhancers, which we anticipate will aid in the rational design of new oral peptide drug formulations in the future.

RESULTS

The mechanism by which a long polar peptide like semaglutide integrates into a membrane while preserving its structural integrity amidst the influence of a permeation enhancer remains an enigmatic process. To investigate this process, we have now made use of all-atom CpHMD simulations (with all the ionizable groups of the peptide and the permeation enhancers treated with a variable protonation state model). Notably, the pK_a values of ionizable sites can change drastically in or near a membrane[2] and/or during complexation/aggregate formation, and CpHMD simulations are an accurate way to capture such environment-dependent effects on the charges of the peptides and the permeation enhancers. Foundational work by the Swanson lab has shown that such effects are key to accurately model the membrane permeation of small-molecule drugs.[2] Yet, prior CpHMD simulations have been limited[26-31] to smaller systems with fewer ionizable functional groups mostly due to unfavorable scaling of the simulation cost with increasing number

of ionizable sites. With the advent of scalable CpHMD models,[26] we have now been able to extend this type of simulation to larger systems. Our work likely represents the largest CpHMD simulation system run to date (with over 400 ionizable functional groups treated at the CpHMD level). Below, the detailed results of these CpHMD simulations are provided together with experimental evidence, all supporting our proposed quicksand-like permeation mechanism for polar peptides.

Free Energy Profiles of SNAC Entering/Exiting a Membrane. Fig. 2B compares the free energy profiles for membrane permeation of SNAC with two different protonation state models: (1) A classical fixed protonation state force field, and (2) the CpHMD-based model. Both models

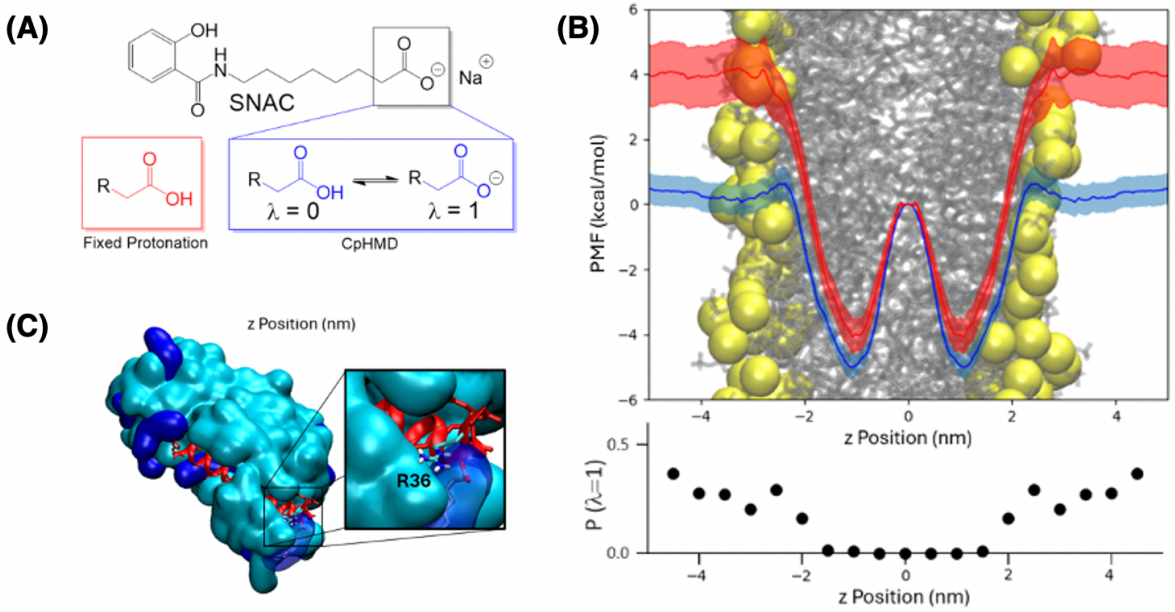

Fig. 2 | Impact of Variable Protonation on the Membrane Insertion of the Permeation Enhancer SNAC. (A) Definition of the λ-coordinate in SNAC for the CpHMD model. **(B)** Potential of mean force (PMF) profiles (310.15 K, 0.15 M NaCl, pH 5) for SNAC insertion into a POPC model membrane (32 lipids per leaflet). The PMF compares a standard, fixed-protonation-state model for protonated SNAC (red curve) to the CpHMD model of SNAC (blue curve). The free energy curve was obtained by umbrella sampling followed by standard WHAM analysis.[1] See Supplementary Movie 1 for the trajectory of the corresponding pulling simulation, which generated the initial frames for the WHAM windows. Shaded bands represent standard error estimates obtained with bootstrapping ($n = 200$) analysis implemented in the GROMACS WHAM analysis software. Z-distance-dependent protonation probabilities were obtained from the CpHMD simulations by binning structures from the WHAM windows based on their z-positions and dividing the number of deprotonated frames by the total number of frames in each bin. **(C)** Self-assembly of 50 SNAC molecules (all treated with the CpHMD model) with semaglutide in aqueous solution after 50 ns (cyan: protonated SNAC ($\lambda < 0.5$); blue: deprotonated SNAC ($\lambda > 0.5$)). See Supplementary Movie 4 for the trajectory of this self-assembly process. The inset highlights an ionic interaction between a deprotonated SNAC molecule and R36 of semaglutide, which illustrates how the peptide environment affects the *p*Ka and with it the dominant protonation state of SNAC.

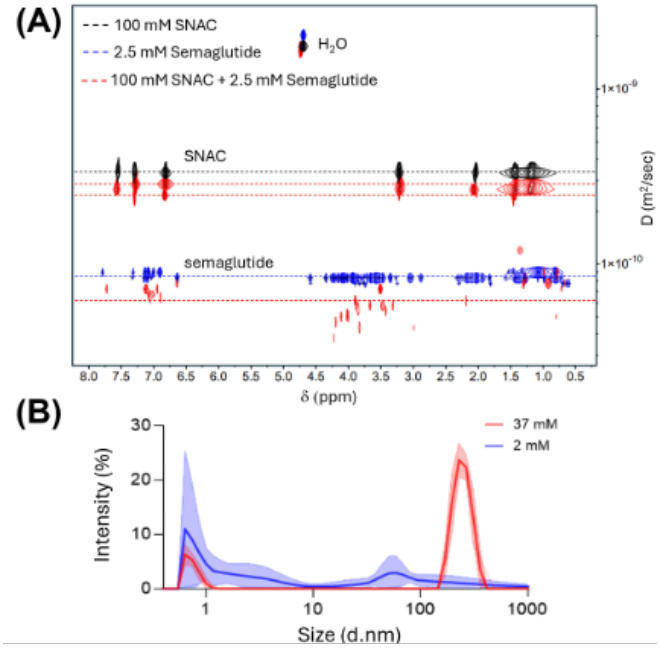

Fig. 3 | Experimental Evidence of SNAC Aggregation in Polar and Non-polar Environments. (A) Stacked convection-compensated ^{1}H DOSY NMR spectra (800 MHz, 298 K, D_2O, pH 7.4 in PBS Buffer, pulse sequence: dstebpg3s) of 100 mM SNAC (black), 2.5 mM semaglutide (blue), and a mixture of 100 mM SNAC and 2.5 mM semaglutide (red). Diffusion coefficients and hydrodynamic radii are detailed in Table 1. **(B)** DLS spectra (298 K, mean intensity ± standard deviation, n = 10) of SNAC in $CDCl_3$ at 37 mM (red) and 2 mM (blue), demonstrating the formation of larger SNAC aggregates in this non-polar environment at the higher concentration. Corresponding correlograms for the DLS spectra are provided in Supplementary Fig. 4.

show SNAC spontaneously incorporating into the membrane, in agreement with prior results obtained with fixed protonation state models.[22] However, with the CpHMD methodology, we now find that SNAC dynamically ionizes in the aqueous phase and then neutralizes to pass through the lipid bilayer membrane (see also Supplementary Fig. 13). This process significantly lowers the free energy for SNAC in the aqueous phase, compared to the aqueous free energy obtained with the corresponding fixed protonation-state force field. The less biased distribution of SNAC between the water and membrane layer obtained with the CpHMD model revealed that SNAC can perform a dual role in monomerizing the peptide and facilitating permeation as described below.

Co-Aggregation of SNAC and Semaglutide in the Aqueous Phase. Next, with a larger CpHMD system containing 50 SNACs in a water box, we found that SNAC rapidly aggregates around semaglutide (Fig. 2C) in water. These simulations also demonstrated that the protonation states of SNAC and semaglutide during co-aggregation are strongly influenced by the interactions between SNAC and semaglutide, as well as interactions with other SNAC molecules. This result further highlights the need for a CpHMD model to capture these dynamic, environment-dependent effects. For instance, a salt bridge was formed between a SNAC molecule and R36 in semaglutide, which

Table 1 | Evidence of SNAC/Semaglutide Co-aggregation in Water Based on Convection-corrected ^{1}H DOSY NMR. The table lists the diffusion coefficients (D) and corresponding hydrodynamic radii (R) of SNAC and semaglutide, calculated with the Stokes-Einstein Equation. The diffusion coefficient of the solvent was used to correct for slight variations in sample viscosity.

Sample	D (m^2 sec^{-1})	R (nm)
100 mM SNAC	3.38×10^{-10}	0.74
2.5 mM semaglutide	8.34×10^{-11}	3.41
100 mM SNAC + 2.5 mM semaglutide	SNAC: 2.79×10^{-10}	0.83
	SNAC:** 2.44×10^{-10}	0.94
	Semaglutide:** 6.17×10^{-11}	3.72

**: We hypothesize that free SNAC and SNAC in the cluster around semaglutide exchange rapidly on the NMR timescale, which leads to distinct diffusion bands for SNAC and semaglutide resonances.

stabilizes the deprotonated state of the corresponding SNAC (Fig. 2C) and significantly lowers the pK$_a$ value of its carboxylic acid function.

To experimentally validate the computationally observed co-association between SNAC and semaglutide, we conducted convection-corrected ^{1}H DOSY NMR experiments with buffered solutions of SNAC, semaglutide, and a 40:1 mixture of the two compounds. Our results (Table 1 and Fig. 3A) indicate that the viscosity-corrected hydrodynamic radii for SNAC and semaglutide increase for both compounds when mixed together. This result is consistent with the computationally observed co-aggregation of the two compounds. Notably, the ^{1}H DOSY NMR signals for SNAC exhibit (Fig. 3A and Table 1) two diffusion coefficients, suggesting that SNAC aggregates of at least two different sizes are formed. Overall, these combined experimental and computational observations provide a direct indication for aggregation between SNAC and semaglutide in the aqueous layer to (1) help monomerize the semaglutide in aqueous solution[6] and (2) improve the affinity of the semaglutide-SNAC aggregates to membrane-bound SNAC aggregates (which we hypothesize helps recruit the semaglutide to the membrane surface as discussed in detail below). See Supplementary Movie 7 for a visual depiction of this process.

Dynamic SNAC Aggregation and Co-Aggregation with Semaglutide in Nonpolar Environments. Individually, SNAC aggregation in aqueous media has been reported.[5, 32] However, SNAC's behavior in non-polar environments is still mostly unknown yet crucial for facilitating the membrane permeation of semaglutide. Our observations now reveal that protonated SNAC also has the potential to aggregate in non-polar environments, as demonstrated by DLS (Fig. 3B) and through CpHMD simulations (Fig. 4). Specifically, the CpHMD simulations show

SNAC forming dynamic aggregates in CH_2Cl_2 (Fig. 4A) as well as inside a model membrane (Figs. 4B/C). The computational model indicates that SNAC aggregation is driven by hydrogen bonding (Fig. 4A and Supplementary Fig. 28), including branched hydrogen bonds that can lead to dynamic network formation inside the membrane.

Experimental evidence for intermolecular hydrogen bonding between SNACs was obtained through a ^{1}H NMR titration of protonated SNAC in $CDCl_3$ (Supplementary Figs. 1 and 2). $CDCl_3$ was chosen as a model system since it is a well-established surrogate for the nonpolar environment of lipid bilayer membranes. [3, 23-25, 33] From these NMR titrations, we found that the amide and

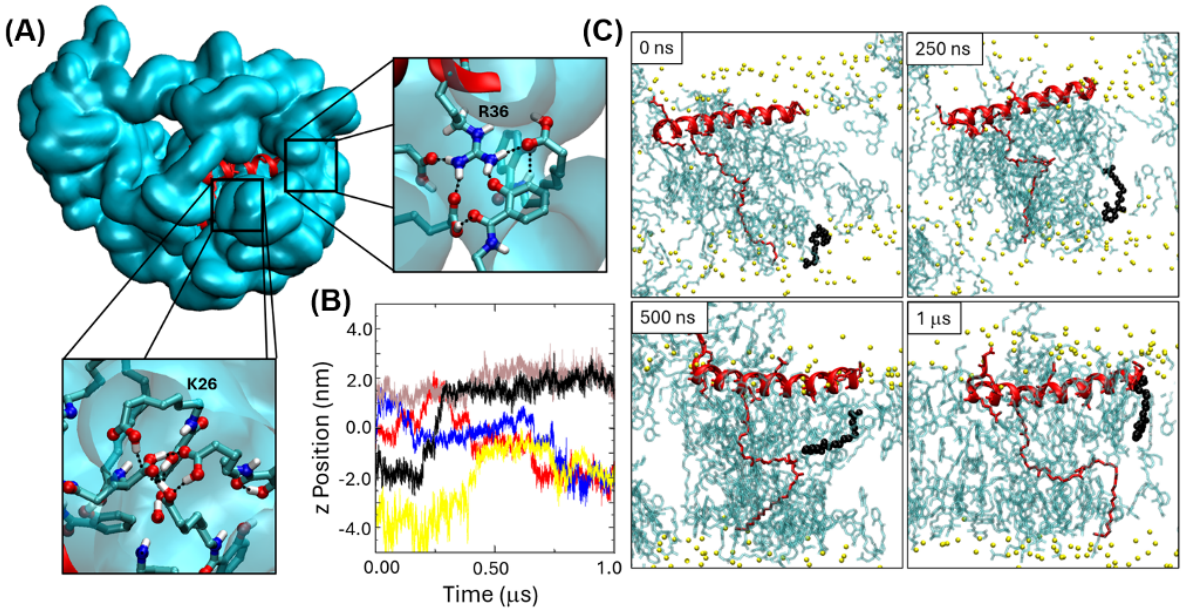

Fig. 4 | Computational Support for Dynamic SNAC Aggregation in Non-polar Environments. (A) Self-assembly of 50 SNAC molecules with semaglutide in CH_2Cl_2 after 50 ns (cyan: protonated SNAC with $\lambda < 0.5$; blue: deprotonated SNAC with $\lambda > 0.5$). The insets highlight stabilizing interactions between SNAC and titratable peptide residues. See Supplementary Fig. 22 for the corresponding aggregation of just SNAC in CH_2Cl_2 and Supplementary Movies 3 and 4 for the corresponding trajectories. **(B)** Time-distance plots showing the z-distance from the membrane center of select SNAC molecules throughout a 1 μs unbiased CpHMD simulation. The z-distance was calculated as the z-component of the distance between the membrane center of mass (phosphate headgroups) and the carboxylic acid carbon atom of the titratable groups of the SNAC molecules. **(C)** Representative snapshots of a model system with semaglutide (red), phosphate head groups (yellow), SNAC (cyan), and a highlighted dynamic SNAC molecule (black, space-filling — color coordinated to match the trace shown in Fig. 4B). The highlighted SNAC molecule moves along the surface of a membrane-bound SNAC aggregate through the membrane to help stabilize semaglutide, illustrating the partially fluid nature of the SNAC aggregates in the membrane. Additional examples with other dynamic SNAC molecules that are part of a membrane cluster are shown in Supplementary Figs. 24–27 and in Supplementary Movie 10.

carboxylic acid resonances of SNAC are highly sensitive to sample concentration, as expected for intermolecular hydrogen bond formation. Specifically, the observed upfield shift of the amide resonance with increasing SNAC concentration is attributed to an increase in hydrogen bonding, which deshields the amide and carboxylic acid peaks.[34] Furthermore, at higher SNAC concentrations (>70 mM), the titration curve deviates significantly from a simple 1:1 binding model (Supplementary Fig. 2), indicating the formation of larger aggregates, which were also observed by DLS (Fig. 2B). Additionally, convection-corrected ^{1}H DOSY NMR spectra show that the diffusion coefficient of SNAC in $CDCl_3$ decreases with increasing SNAC concentration (Supplementary Fig. 3), which is also consistent with SNAC aggregate formation.

Based on the measured diffusion coefficients and assuming spherical aggregates, the average aggregate volumes for 5 mM and 100 mM samples of protonated SNAC in $CDCl_3$ (298 K) were calculated to be 0.42 nm³ and 1.05 nm³, respectively, using the Stokes-Einstein relationship.[35] Even larger SNAC aggregates (~150 nm diameter) were observed by DLS in $CDCl_3$ (Fig. 3B), which is more sensitive to larger particles than NMR.[36] Overall, the experimentally observed aggregation of SNAC in $CDCl_3$ supports our computational results, which show that dynamic SNAC aggregates can form in CH_2Cl_2 as well as in the interior of a lipid bilayer membrane. The dynamic nature of the SNAC aggregates in the membrane is demonstrated in Figs. 4B and 4C, as well as in Supplementary Figs. 24–28 and Supplementary Movie 10, which all highlight the significant movement of selected SNAC molecules in the membrane (all of them part of SNAC membrane clusters) during a 1-μs CpHMD simulation.

Spontaneous Incorporation of Semaglutide into the Membrane in the Presence of SNAC. To directly observe the mechanism of peptide permeation in the presence of SNAC computationally, we performed unbiased CpHMD simulations with a system containing 400 SNAC molecules (periodic box size: 11 nm x 11 nm x 15 nm), semaglutide, and a model POPC/cholesterol epithelial membrane (see Fig. 5A). Semaglutide and SNAC were randomly placed around the membrane, and the system was run for 100 ns to equilibrate. The membrane was constructed using Packmol,[37] with its composition based on estimates of the cholesterol content in epithelial cells[38, 39] and previously reported simulations of SNAC.[40, 41] During the first 5 ns, semaglutide once again rapidly aggregated with neighboring SNAC molecules in the aqueous layer. Subsequently, semaglutide clusters in the water layer spontaneously fused with a membrane-bound SNAC aggregate,

positioning the peptide flat on the membrane surface after ~50 ns. Similar synergistic aggregation mechanisms have been described previously for antimicrobial peptides.[42]

Next, given its hydrophobic nature, we hypothesized that the lipid tail of semaglutide (which includes[43, 44] the fatty acid chain and γGlu-2xOEG linker ligated to K26 as shown in Supplementary Figs. 5 and 6) likely inserts first into the membrane, serving as a membrane anchor for the peptide. To confirm this hypothesis, we calculated the free energy profile for membrane insertion of the semaglutide lipid tail with the CpHMD method, using umbrella sampling followed by WHAM analysis[45] (Supplementary Figs. 16–18). Our results showed that incorporating the lipid tail anchor into the membrane center is favorable overall (ΔG = –4.8 kcal mol^{-1}). However, pulling the acid end of the lipid tail to the opposite leaflet imposed an 8.2 kcal mol^{-1} free energy barrier due to the γGlu-2xOEG linker being pulled past the phosphate headgroups. Based on these results, we constructed an initial structure with the lipid tail of semaglutide anchored inside the

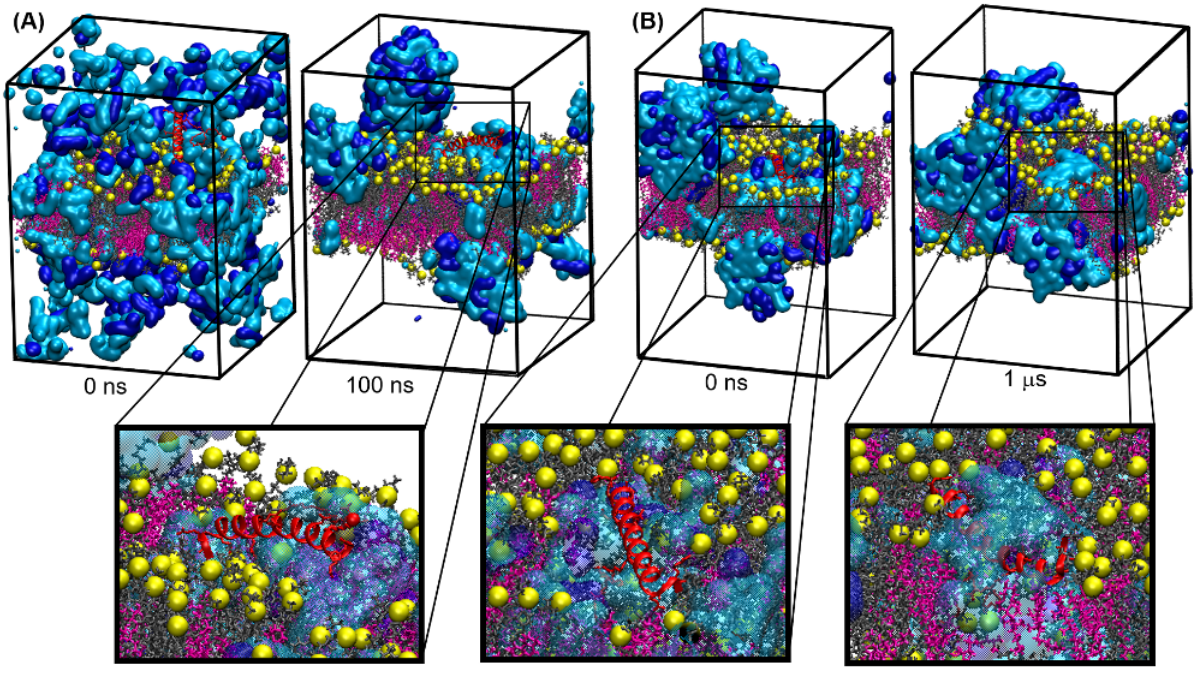

Fig. 5 | Unbiased CpHMD Simulations Showing Semaglutide Spontaneously Adhering to and Incorporating into the Membrane in the Presence of SNAC. The model contained semaglutide (red), 60% POPC lipids (yellow/grey), 40% cholesterol (pink), and 400 SNAC molecules (cyan: protonated with λ < 0.5; blue: deprotonated with λ > 0.5). **(A)** 100-ns CpHMD simulation during which a SNAC-semaglutide aggregate spontaneously forms and adsorbs to the membrane surface. **(B)** 1-μs CpHMD simulation, which was started from a snapshot with semaglutide's fatty acid tail anchored in the membrane. After a few hundred nanoseconds semaglutide spontaneously starts to sink into the SNAC defects formed inside the membrane as the peptide drug is getting buried by SNAC molecules moving from the center of the membrane toward the semaglutide. Videos of these trajectories are included as Supplementary Movies 6–9.

membrane for extended, 1-μs unbiased CpHMD simulations of this system as shown in Fig. 5B.[46]

As this simulation progressed (see Supplementary Movie 8 for a visual depiction of this process), the initial, smaller SNAC aggregates gradually expanded within the membrane, forming larger SNAC-filled membrane defects spanning the phospholipid head groups (Supplementary Fig. 21). Additional SNAC then continued to aggregate around the membrane-anchored peptide, which began to slowly sink into the membrane after ~100 ns. Throughout the remainder of this unbiased simulation, semaglutide continued to sink into the membrane as more SNAC molecules enveloped the hydrophobic portions of the peptide (see Figs. 1C, 5B, and Supplementary Movie 8). Based on these results, we hypothesize that — as semaglutide sinks through the SNAC membrane defects — there is a dynamic redistribution of the surrounding SNAC molecules. Specifically, SNACs located near the exterior of the membrane-bound defects are more dynamic than those in the interior of the defects (see Figs. 4C and Supplementary Figs. 24–27). This movement of mobile SNACs along the exterior of the dynamic defects gradually sinks the peptide into the membrane. Then, as new SNACs are exposed to the exterior of the defects, they once again move to the top of the cluster, continuing the sinking process. This proposed mechanism, which resembles sinking into quicksand, is illustrated with curved arrows in Fig. 6.

DISCUSSION

With a combination of molecular dynamics simulations and experimental methods, we have, for the first time, observed how a polar peptide like semaglutide can spontaneously sink into a membrane in the presence of a permeation enhancer (SNAC), to get delivered across the intestinal barrier. Dynamic protonation of weakly ionizable sites is crucial for this process, which we were able to observe with a CpHMD model that can accurately represent the environment- and aggregation-/conformation-dependent charges in this system. While dynamic protonation of ionizable sites is well-known to influence biological processes[27, 28, 30, 47-51] and membrane permeability for small molecules (see Fig. 1A for a seminal example),[2, 52-56] this work has now advanced the application of CpHMD models to permeation-enhancer facilitated peptide permeation by treating all the permeation enhancers and all ionizable sites on a peptide drug (>400 ionizable groups in total) with a CpHMD model.

Furthermore, while both SNAC and semaglutide are known to form aggregates by themselves in

buffered aqueous solutions based on DLS and DOSY NMR,[32, 57] our CpHMD simulations have now clearly demonstrated co-association of the peptide with the permeation enhancer in the aqueous phase. We hypothesize that this observed co-aggregation is primarily responsible for the previously reported monomerization[6] of the peptide drug in an aqueous buffer in the presence of SNAC, a mechanism that was previously unknown.[5] In addition, since we found a clear affinity of SNAC toward itself and semaglutide in both aqueous and hydrophobic environments, the co-aggregation of SNAC with semaglutide might also play an important role in helping to recruit the SNAC-bound semaglutide from the aqueous layer to the membrane (with the SNAC around the semaglutide fusing with membrane-bound SNAC). Based on our combined computational and experimental results, we propose the overall mechanism shown in Figure 6 for peptide permeation with SNAC. Key steps include:

(1) Excess SNAC around the tablet forms aggregates with semaglutide and the membrane.

(2) SNAC molecules leave the aqueous cluster one at a time, incorporating into the membrane to form dynamic, SNAC-filled membrane defects, which allow semaglutide to bypass the phosphate head group barrier.

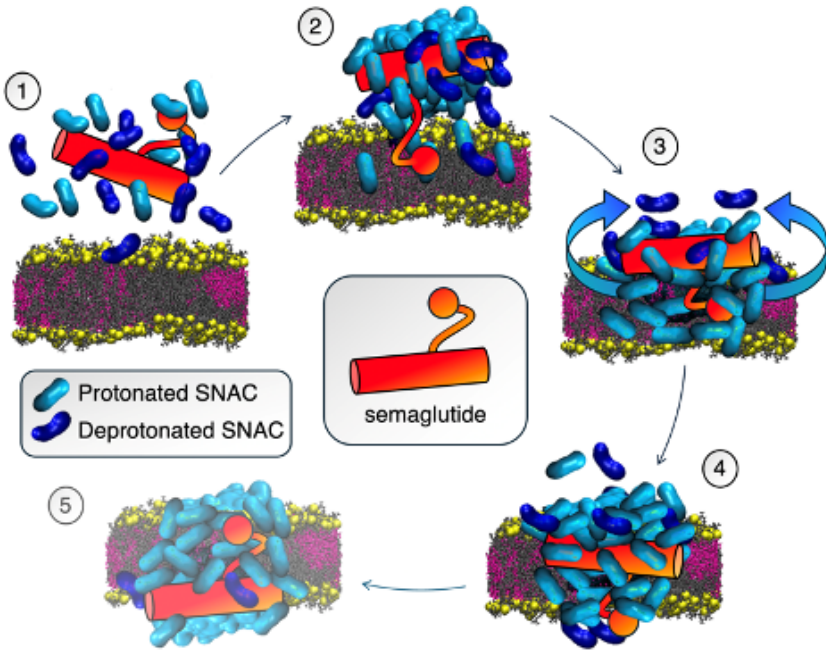

Fig. 6 | Hypothesized Molecular Mechanism for SNAC-Assisted Membrane Permeation of Semaglutide. Steps 1–4 are directly supported by the results presented in this work, while step 5 remains hypothetical.

(3) Solution-based semaglutide-SNAC aggregates fuse with dynamic, membrane-bound SNAC-filled membrane defects, adsorbing semaglutide onto the membrane surface.

(4) The fatty acid chain of semaglutide anchors the peptide to the membrane, with SNAC

molecules in the membrane creating a "quicksand-like" effect enabling the peptide to sink into the membrane.

(5) The peptide keeps sinking through the dynamic SNAC-filled membrane defects until it reaches the other side of the membrane, where it then exits with excess SNAC maintaining membrane integrity after peptide passage.

In summary, our CpHMD model revealed SNAC's dual role in peptide membrane permeation. First, in the water layer, SNAC associates with semaglutide, acting as a surfactant to help monomerize the peptide while remaining partially deprotonated. Second, upon membrane insertion, SNAC neutralizes and forms dynamic, hydrogen bond-driven membrane defects to help facilitate membrane permeation of the peptide drug. Our proposed mechanism for the passive membrane permeation of semaglutide is unprecedented, being the first to be substantiated by accurate CpHMD atomistic models (with all weakly ionizable functional groups in both the peptide and all the permeation enhancers modeled with CpHMD). While it delineates one of numerous potential pathways for semaglutide to traverse a membrane in the presence of SNAC,[58, 59] the integration of scalable CpHMD elevates it to one of the most expansive and accurate models documented to date. Moreover, the overarching principles elucidated in this study — specifically, SNAC's behavior in nonpolar environments, its dynamic aggregation with semaglutide in both polar and nonpolar contexts, and the formation of SNAC-filled dynamic defects within the membrane — present foundational concepts, which hold significant potential to inform and refine the development of novel peptide drug/permeation enhancer combinations in the future. The adhesion of semaglutide to the membrane, which was observed in our CpHMD simulations, also agrees with the initial steps for cell translocation of known cell-penetrating peptides.[60] Overall, our results provide a new viable mechanism for cell permeation to help advance the field of oral peptide drug delivery, including potentially for macrocyclic peptides in the future.[3, 61-63]

METHODS

CpHMD Simulations. The simulations described in this work utilized a scalable CpHMD method implemented by the Groenhof and Hess groups in a custom fork of GROMACS 2021.[26] Due to the environment and conformation-dependent pK_a values of all the weakly ionizable functional

groups in the peptide and the SNACs, the enhanced accuracy of a CpHMD model is crucial to meaningfully predict the charges and interactions between semagtlutide, SNAC, and the membrane.[29] Specifically, we found that the charges of the permeation enhancers and the peptides (which are directly controlled by the protonation states) are highly environment-dependent, which significantly affects the free energy change associated with membrane insertion of SNAC (Fig. 2A). In this work, the CpHMD model enabled the simulation of all the titratable sites in the peptide and ~400 permeation enhancers under constant pH conditions at ~80% of the efficiency of standard MD simulations.[26] The 400:1 molar ratio of SNAC:semaglutide in the simulations was chosen based on the current formulations in Rybelsus,[64] which contains ~1 mmol of SNAC per tablet in a ~300:1 to ~1300:1 SNAC:semaglutide molar ratio).

To enable these large-scale CpHMD simulations, we first generated CpHMD parameters for the titratable groups of SNAC and non-standard amino acids following standard best practices as detailed in the Supplemental Methods section.[31] All of our CpHMD parameters are provided in Supplementary Table 1 and Supplementary Figs. 8–13. Furthermore, to mimic the localized SNAC-buffered environment around the tablet, which is less acidic than the rest of the stomach,[5] the CpHMD simulations were performed at pH = 5.0 (the pK_a value of SNAC in water).[65] Additional details regarding all the CpHMD parametrizations and simulations performed are provided in the Supplementary Methods section.

^{1}H NMR Titrations of SNAC. SNAC was dissolved in 0.7 mL $CDCl_3$ containing 1% (v/v) TMS at concentrations ranging from 5 mM to 100 mM with gentle heating. Spectra were recorded immediately after the samples were dissolved on a Bruker NOE500-2 spectrometer for 32 scans at 298 K and all resonances were referenced to TMS as the internal standard. Clear concentration-dependent shifts (Supplementary Fig. 1) of the amide (N-H) resonance in SNAC at ~6.3 ppm were observed, which is indicative of attractive supramolecular interactions dominated by hydrogen bonding (shown in Supplementary Fig. 28) between the SNAC molecules in $CDCl_3$ solution. The resulting ^{1}H NMR chemical shift-concentration plots (Supplementary Fig. 2) were then analyzed with the with the Dynafit[66] (v 4.11.110) software package using a simple 1:1 homodimerization binding model for SNAC concentrations < 70 mM. However, for larger SNAC concentrations, clear deviations from a simple 1:1 binding model were observed, which is consistent with the formation of larger, dynamic SNAC aggregates that are also observed in DLS (Fig. 3B) and by all-

atom molecular dynamics simulations (Fig. 4 and Supplementary Fig. 21).

^{1}H Diffusion-ordered Spectroscopy (DOSY) NMR. The NMR samples for ^{1}H DOSY NMR spectroscopy were prepared in $CDCl_3$ (0.3 mL) at 298 K and recorded with chloroform-*d*-matched Shigemi NMR tubes (Wilmad CMS-005B) to minimize convection. The caps of the NMR tubes were sealed with parafilm before being lowered into the magnet. The ^{1}H DOSY NMR spectra were acquired on a Bruker Avance-lll-800 (800 MHz) spectrometer with a standard-bore Bruker ultra stabilized magnet, equipped with a 5mm QCI Z-gradient cryoprobe containing a cold ^{13}C preamp, a Z-axis field gradient module, four RF channels with waveform generation, H2-decoupling capability, a sample temperature control unit, and a Linux host computer running TopSpin 4.1.1. The DOSY pulse program used was a standard double-stimulated-echo experiment with bipolar gradient pulses and convection compensation (Pulse Sequence: dstebpg3s implemented in TopSpin). A total of 16 different spectra were recorded for all samples using a 98% pulse gradient for SNAC/SNAC and 69% pulse gradient for semaglutide, and data were processed in MestReNova (v 14.3.3) using the Peak Fit method. The hydrodynamic radii were estimated using the Stokes-Einstein equation. This equation was solved for R (the solvodynamic radius) using appropriate values for the solvent viscosity η from the literature.

Dynamic Light Scattering (DLS). Samples were prepared by dissolving protonated SNAC in $CDCl_3$ (Cambridge Isotopes Cat. No.: DLM-29-0) in 15 mL scintillation vials with gentle heating. The dissolved samples were then filtered through celite and transferred to an ultra-low volume quartz cuvette (ZEN2112) for the acquisition of the DLS spectra. The concentration of the samples was quantified with ^{1}H NMR after filtration through celite. Quantitation was performed with 1,3,5-tribromobenzene as the internal standard and the $D1$ NMR acquisition delay parameter in Topspin was set to 10 s to ensure accurate NMR integrations. For DLS spectrum acquisition, each DLS spectrum was recorded 10 times. Samples were given 15 seconds to equilibrate in between the different measurements.

Data availability. The data that support the findings of this study are available within Supplementary Information files and are also available from the corresponding author upon reasonable request.

REFERENCES AND NOTES

(1) Hub, J. S.; de Groot, B. L.; van der Spoel, D. G_Wham: A Free Weighted Histogram Analysis Implementation Including Robust Error and Autocorrelation Estimates. *J. Chem. Theory Comput.* **2010**, *6*, 3713–3720.

(2) Yue, Z.; Li, C.; Voth, G. A.; Swanson, J. M. J. Dynamic Protonation Dramatically Affects the Membrane Permeability of Drug-like Molecules. *J. Am. Chem. Soc.* **2019**, *141*, 13421–13433.

(3) Bhardwaj, G.; O'Connor, J.; Rettie, S.; Huang, Y. H.; Ramelot, T. A.; Mulligan, V. K.; Alpkilic, G. G.; Palmer, J.; Bera, A. K.; Bick, M. J.; *et al.* Accurate *De Novo* Design of Membrane-traversing Macrocycles. *Cell* **2022**, *185*, 3520–3532.

(4) Venable, R. M.; Kramer, A.; Pastor, R. W. Molecular Dynamics Simulations of Membrane Permeability. *Chem. Rev.* **2019**, *119*, 5954–5997.

(5) Ahnfelt-Roenne, J.; Madsen, K. G.; Scheele, S. G.; Alanentalo, T.; Kirk, R. K.; Pedersen, B. L.; Skyggebjerg, R. B.; Benie, A. J.; Strauss, H. M.; Wahlund, P.-O.; *et al.* Transcellular Stomach Absorption of a Derivatized Glucagon-like Peptide-1 Receptor Agonist. *Sci. Transl. Med.* **2018**, *10*, eaar7047/7041.

(6) Aroda, V. R.; Blonde, L.; Pratley, R. E. A New Era for Oral Peptides: SNAC and the Development of Oral Semaglutide for the Treatment of Type 2 Diabetes. *Rev. Endocr. Metab. Disord.* **2022**, *23*, 979–994.

(7) Bucheit, J. D.; Pamulapati, L. G.; Carter, N.; Malloy, K.; Dixon, D. L.; Sisson, E. M. Oral Semaglutide: A Review of the First Oral Glucagon-Like Peptide 1 Receptor Agonist. *Diabetes Technol. Ther.* **2020**, *22*, 10–18.

(8) Kommineni, N.; Sainaga Jyothi, V. G. S.; Butreddy, A.; Raju, S.; Shapira, T.; Khan, W.; Angsantikul, P.; Domb, A. J. SNAC for Enhanced Oral Bioavailability: An Updated Review. *Pharm. Res.* **2023**, *40*, 633–650.

(9) Wong, N. D.; Karthikeyan, H.; Fan, W. US Population Eligibility and Estimated Impact of Semaglutide Treatment on Obesity Prevalence and Cardiovascular Disease Events. *Cardiovasc. Drugs Ther.* **2023**, DOI: 10.1007/s10557-023-07488-3.

(10) Chen, G.; Kang, W.; Li, W.; Chen, S.; Gao, Y. Oral Delivery of Protein and Peptide Drugs: Fromnon-specific Formulation Approaches to Intestinal Cell Targeting Strategies. *Theranostics* **2022**, *12*, 1419–1439.

(11) Ismail, R.; Csoka, I. Novel Strategies in the Oral Delivery of Antidiabetic Peptide Drugs — Insulin, GLP 1 and Its Analogs. *Eur. J. Pharm. Biopharm.* **2017**, *115*, 257–267.

(12) Li, Y.; Zhang, W.; Zhao, R.; Zhang, X. Advances in Oral Peptide Drug Nanoparticles for Diabetes Mellitus Treatment. *Bioact. Mater.* **2022**, *15*, 392–408.

(13) Muttenthaler, M.; King, G. F.; Adams, D. J.; Alewood, P. F. Trends in Peptide Drug Discovery. *Nat. Rev. Drug Discovery* **2021**, *20*, 309–325.

(14) Overgaard, R. V.; Navarria, A.; Ingwersen, S. H.; Baekdal, T. A.; Kildemoes, R. J. Clinical Pharmacokinetics of Oral Semaglutide: Analyses of Data from Clinical Pharmacology Trials. *Clin. Pharmacokinet.* **2021**, *60*, 1335–1348.

(15) Anselmo, A. C.; Gokarn, Y.; Mitragotri, S. Non-invasive Delivery Strategies for Biologics. *Nat. Rev. Drug Discovery* **2019**, *18*, 19–40.

(16) Renukuntla, J.; Vadlapudi, A. D.; Patel, A.; Boddu, S. H. S.; Mitra, A. K. Approaches for Enhancing Oral Bioavailability of Peptides and Proteins. *Int. J. Pharm.* **2013**, *447*, 75–93.

(17) Drucker, D. J. Advances in Oral Peptide Therapeutics. *Nat. Rev. Drug Discovery* **2020**, *19*, 277–289.

(18) McCartney, F.; Gleeson, J. P.; Brayden, D. J. Safety Concerns Over the use of Intestinal Permeation Enhancers: A Mini-review. *Tissue Barriers* **2016**, *4*, e1176822.

(19) Solis-Herrera, C.; Kane, M. P.; Triplitt, C. Current Understanding of Sodium *N*-(8-[2-Hydroxylbenzoyl] Amino) Caprylate (SNAC) as an Absorption Enhancer: The Oral Semaglutide Experience. *Clin. Diabetes* **2024**, *42*, 74–86.

(20) Twarog, C.; Liu, K.; O'Brien, P. J.; Dawson, K. A.; Fattal, E.; Illel, B.; Brayden, D. J. A Head-to-head Caco-2 Assay Comparison of the Mechanisms of Action of the Intestinal Permeation Enhancers: SNAC and Sodium Caprate (C10). *Eur. J. Pharm. Biopharm.* **2020**, *152*, 95–107.

(21) Schneebeli, S. T.; Nie, D.; Colston, K. J.; Li, J. New Insight Into the Oral Delivery Mechanism of Semaglutide Based on All-Atom Molecular Dynamics Simulations. *Proceedings of the PHARMSCI 360 Conference*, Orlando, FL, October 2023,

(22) Kang, C.; Bernaldez, M.; Stamatis, S. D.; Rose, J. P.; Sun, R. Interaction Between Permeation Enhancers and Lipid Bilayers. *J. Phys. Chem. B* **2024**, *128*, 1668–1679.

(23) Naylor, M. R.; Ly, A. M.; Handford, M. J.; Ramos, D. P.; Pye, C. R.; Furukawa, A.; Klein, V. G.; Noland, R. P.; Edmondson, Q.; Turmon, A. C.; *et al.* Lipophilic Permeability Efficiency Reconciles the Opposing Roles of Lipophilicity in Membrane Permeability and Aqueous Solubility. *J. Med. Chem.* **2018**, *61*, 11169–11182.

(24) Ono, S.; Naylor, M. R.; Townsend, C. E.; Okumura, C.; Okada, O.; Lokey, R. S. Conformation and Permeability: Cyclic Hexapeptide Diastereomers. *J. Chem. Inf. Model.* **2019**, *59*, 2952–2963.

(25) Damjanovic, J.; Miao, J.; Huang, H.; Lin, Y.-S. Elucidating Solution Structures of Cyclic Peptides Using Molecular Dynamics Simulations. *Chem. Rev.* **2021**, *121*, 2292–2324.

(26) Aho, N.; Buslaev, P.; Jansen, A.; Bauer, P.; Groenhof, G.; Hess, B. Scalable Constant pH Molecular Dynamics in GROMACS. *J. Chem. Theory Comput.* **2022**, *18*, 6148–6160.

(27) Henderson, J. A.; Shen, J. Exploring the pH- and Ligand-Dependent Flap Dynamics of Malarial Plasmepsin II. *J. Chem. Inf. Model.* **2022**, *62*, 150–158.

(28) Ma, S.; Henderson, J. A.; Shen, J. Exploring the pH-Dependent Structure-Dynamics-Function Relationship of Human Renin. *J. Chem. Inf. Model.* **2021**, *61*, 400–407.

(29) Martins de Oliveira, V.; Liu, R.; Shen, J. Constant pH molecular dynamics simulations: Current Status and Recent Applications. *Curr. Opin. Struct. Biol.* **2022**, *77*, 102498.

(30) Shen, M.; Huang, Y.; Cai, Z.; Cherny, V. V.; DeCoursey, T. E.; Shen, J. Interior pH-sensing Residue of Human Voltage-gated Proton Channel Hv1 is Histidine 168. *Biophys. J.* **2024**, Published Online, DOI: 10.1016/j.bpj.2024.07.027.

(31) Buslaev, P.; Aho, N.; Jansen, A.; Bauer, P.; Hess, B.; Groenhof, G. Best Practices in Constant pH MD Simulations: Accuracy and Sampling. *J. Chem. Theory Comput.* **2022**, *18*, 6134–6147.

(32) Twarog, C.; Fattal, E.; Noiray, M.; Illel, B.; Brayden, D. J.; Taverna, M.; Hillaireau, H. Characterization of the Physicochemical Interactions Between Exenatide and Two Intestinal Permeation Enhancers: Sodium Caprate (C10) and Salcaprozate Sodium (SNAC). *Int. J. Pharm.* **2022**, *626*, 122131.

(33) Kessler, H.; Kock, M.; Wein, T.; Gehrke, M. Reinvestigation of the Conformation of Cyclosporin A in Chloroform. *Helv. Chim. Acta* **1990**, *73*, 1818.

(34) Wash, P. L.; Maverick, E.; Chiefari, J.; Lightner, D. A. Acid-Amide Intermolecular Hydrogen Bonding. *J. Am. Chem. Soc.* **1997**, *119*, 3802–3806.

(35) The diffusion coefficient of the solvent peak remained nearly identical for the two SNAC solutions in $CDCl_3$ (2.68 x 10^{-9} m^2 s^{-1} for the 5 mM solution and 2.71 x 10^{-9} m^2 s^{-1} for the 100 mM solution), ruling out significant viscosity effects on the apparent diffusion coefficients of SNAC at different concentrations.

(36) Stetefeld, J.; McKenna, S. A.; Patel, T. R. Dynamic Light Scattering: A Practical Guide and Applications in Biomedical Sciences. *Biophys. Rev.* **2016**, *8*, 409–427.

(37) Martinez, L.; Andrade, R.; Birgin, E. G.; Martinez, J. M. PACKMOL: A Package for Building Initial Configurations for Molecular Dynamics Simulations. *J. Comput. Chem.* **2009**, *30*, 2157–2164.

(38) van Ijzendoorn, S. C. D.; Agnetti, J.; Gassama-Diagne, A. Mechanisms Behind the Polarized Distribution of Lipids in Epithelial Cells. *Biochim. Biophys. Acta, Biomembr.* **2020**, *1862*, 183145.

(39) Barbera, N.; Levitan, I. Chiral Specificity of Cholesterol Orientation Within Cholesterol Binding Sites in Inwardly Rectifying K^+ Channels. *Adv. Exp. Med. Biol.* **2019**, *1115*, 77–95.

(40) Kneiszl, R.; Hossain, S.; Larsson, P. In Silico-Based Experiments on Mechanistic Interactions between Several Intestinal Permeation Enhancers with a Lipid Bilayer Model. *Mol. Pharmaceutics* **2022**, *19*, 124–137.

(41) Hossain, S.; Joyce, P.; Parrow, A.; Joemetsa, S.; Hoeoek, F.; Larsson, P.; Bergstroem, C. A. S. Influence of Bile Composition on Membrane Incorporation of Transient Permeability Enhancers. *Mol. Pharmaceutics* **2020**, *17*, 4226–4240.

(42) Remington, J. M.; Liao, C.; Sharafi, M.; Ste. Marie, E. J.; Ferrell, J. B.; Hondal, R. J.; Wargo, M. J.; Schneebeli, S. T.; Li, J. Aggregation State of Synergistic Antimicrobial Peptides. *J. Phys. Chem. Lett.* **2020**, *11*, 9501–9506.

(43) Knudsen, L. B.; Lau, J. The Discovery and Development of Liraglutide and Semaglutide. *Front Endocrinol.* **2019**, *10*, 155.

(44) Mahapatra, M. K.; Karuppasamy, M.; Sahoo, B. M. Semaglutide, a Glucagon-like Peptide-1 Receptor Agonist with Cardiovascular Benefits for Management of Type 2 Diabetes. *Rev. Endocr. Metab. Disord.* **2022**, *23*, 521–539.

(45) Grossfield, A. Grossfield, Alan, "WHAM: The Weighted Histogram Analysis Method", Version 2.0.11, http://membrane.urmc.rochester.edu/wordpress/?page_id=126. Accessed: July 2024.

(46) This simulation was repeated with a different random seed, which yielded very similar results, and also showed the peptide spontaneously sinking into the SNAC-filled membrane defects.

(47) Yue, Z.; Bernardi, A.; Li, C.; Mironenko, A. V.; Swanson, J. M. J. Toward a Multipathway Perspective: pH-Dependent Kinetic Selection of Competing Pathways and the Role of the Internal Glutamate in Cl^-/H^+ Antiporters. *J. Phys. Chem. B* **2021**, *125*, 7975–7984.

(48) Weber, R.; McCullagh, M. The Role of Hydrophobicity in the Stability and pH-Switchability of $(RXDX)_4$ and Coumarin-$(RXDX)_4$ Conjugate β-Sheets. *J. Phys. Chem. B* **2020**, *124*, 1723–1732.

(49) Liang, C.; Savinov, S. N.; Fejzo, J.; Eyles, S. J.; Chen, J. Modulation of Amyloid-β42 Conformation by Small Molecules Through Nonspecific Binding. *J. Chem. Theory Comput.* **2019**, *15*, 5169–5174.

(50) Davidson, R. B.; Hendrix, J.; Geiss, B. J.; McCullagh, M. RNA-dependent Structures of the RNA-binding Loop in the Flavivirus NS3 Helicase. *J. Phys. Chem. B* **2020**, *124*, 2371–2381.

(51) Nordquist, E. B.; Clerico, E. M.; Chen, J.; Gierasch, L. M. Computationally-Aided Modeling of Hsp70-Client Interactions: Past, Present, and Future. *J. Phys. Chem. B* **2022**, *126*, 6780–6791.

(52) Kang, C.; Shoji, A.; Chipot, C.; Sun, R. Impact of the Unstirred Water Layer on the Permeation of Small-Molecule Drugs. *J. Chem. Inf. Model.* **2024**, *64*, 933–943.

(53) Sun, R.; Han, Y.; Swanson, J. M. J.; Tan, J. S.; Rose, J. P.; Voth, G. A. Molecular Transport Through Membranes: Accurate Permeability Coefficients from Multidimensional Potentials of Mean Force and Local Diffusion Constants. *J. Chem. Phys.* **2018**, *149*, 072310/072311.

(54) Sun, R.; Dama, J. F.; Tan, J. S.; Rose, J. P.; Voth, G. A. Transition-Tempered Metadynamics Is a Promising Tool for Studying the Permeation of Drug-like Molecules through Membranes. *J. Chem. Theory Comput.* **2016**, *12*, 5157–5169.

(55) Shoji, A.; Kang, C.; Fujioka, K.; Rose, J. P.; Sun, R. Assessing the Intestinal Permeability of Small Molecule Drugs via Diffusion Motion on a Multidimensional Free Energy Surface. *J. Chem. Theory Comput.* **2022**, *18*, 503–515.

(56) Oh, M.; da Hora, G. C. A.; Swanson, J. M. J. tICA-Metadynamics for Identifying Slow Dynamics in Membrane Permeation. *J. Chem. Theory Comput.* **2023**, *19*, 8886–8900.

(57) Wang, K.; Chen, K. Direct Assessment of Oligomerization of Chemically Modified Peptides and Proteins in Formulations using DLS and DOSY-NMR. *Pharm. Res.* **2023**, *40*, 1329–1339.

(58) Kim, J. C.; Park, E. J.; Na, D. H. Review on Gastrointestinal Permeation Enhancers for Development of Oral Peptide Pharmaceuticals. *Pharmaceuticals* **2022**, *15*, 1585.

(59) Maher, S.; Brayden, D. J. Formulation Strategies to Improve the Efficacy of Intestinal Permeation Enhancers. *Adv. Drug Delivery Rev.* **2021**, *177*, 113925.

(60) Sahni, A.; Ritchey, J. L.; Qian, Z.; Pei, D. Cell-Penetrating Peptides Translocate across the Plasma Membrane by Inducing Vesicle Budding and Collapse. *J. Am. Chem. Soc.* **2024**. Published Online, DOI: 10.1021/jacs.4c10533.

(61) Dougherty, P. G.; Sahni, A.; Pei, D. Understanding Cell Penetration of Cyclic Peptides. *Chem. Rev.* **2019**, *119*, 10241–10287.

(62) Linker, S. M.; Schellhaas, C.; Kamenik, A. S.; Veldhuizen, M. M.; Waibl, F.; Roth, H. J.; Fouche, M.; Rodde, S.; Riniker, S. Lessons for Oral Bioavailability: How Conformationally Flexible Cyclic Peptides Enter and Cross Lipid Membranes. *J. Med. Chem.* **2023**, *66*, 2773–2788.

(63) Bohley, M.; Leroux, J. C. Gastrointestinal Permeation Enhancers Beyond Sodium Caprate and SNAC — What is Coming Next? *Adv. Sci.* **2024**, e2400843. DOI: 10.1002/advs.202400843.

(64) *Rybelsus® (semaglutide tablest) Product Monograph*; Rev. 267692; NovoNordisk, March 30, 2020.

(65) Fattah, S.; Ismaiel, M.; Murphy, B.; Rulikowska, A.; Frias, J. M.; Winter, D. C.; Brayden, D. J. Salcaprozate Sodium (SNAC) Enhances Permeability of Octreotide Across Isolated Rat and Human Intestinal Epithelial Mucosae in Ussing Chambers. *Eur. J. Pharm. Sci.* **2020**, *154*, 105509.

(66) Kuzmic, P. "Program DYNAFIT for the Analysis of Enzyme Kinetic Data: Application to HIV Proteinase" *Anal. Biochem.* **1996**, *237*, 260–273.

END NOTES

Acknowledgements. We thank Dr. Huaping Mo for assistance with DOSY NMR spectroscopy, Dr. Jianing Li for helpful discussions, the Purdue Rosen Center for Advanced Computing for providing computational facilities, and the Purdue Interdepartmental NMR Facility for providing access to NMR spectrometers used to carry out this research. We thank the NIH for funding this work under a MIRA grant awarded to S.T.S. (1R35GM147579). Part of the computational resources were also supported by an NSF CAREER Award (CHE-1848444/2317652). Finally, we would also like to acknowledge the use of artificial intelligence tools (Microsoft Copilot) to enhance the conciseness and clarity of some of the writing in this paper.

Author contributions. S.T.S. guided the project, discussed the experimental and computational results, and helped write the paper. K.J.C. performed and analyzed the simulations and part of the experiments reported in the paper. K.T.F. performed and analyzed part of the experiments reported in the paper. All the authors discussed the results and revised the paper.

Competing financial interests. The authors declare no competing financial interests.